Resonant states and pseudospin symmetry in the Dirac-Morse potential

Quan Liu, Zhong-Ming Niu, and Jian-You Guo[*]

School of Physics and Material Science, Anhui University, Hefei 230039, People's Republic of China
(Received 29 January 2013; published 16 May 2013)

The complex scaling method is applied to study the resonances of a Dirac particle in a Morse potential. The applicability of the method is demonstrated with the results compared with the available data. It is shown that the present calculations in the nonrelativistic limit are in excellent agreement with the nonrelativistic calculations. Further, the dependence of the resonant parameters on the shape of the potential is checked with the sensitivity to the potential parameters analyzed. By comparing the energies and widths of the pseudospin doublets, well pseudospin symmetry is discovered in the present model. The relationship between the pseudospin symmetry and the shape of the potential is investigated by changing the Morse potential shaped by the dissociation energy, the equilibrium intermolecular distance, and the positive number controlling the decay length of the potential.

PACS number(s): 03.65.Pm, 33.15.Bh, 34.20.Gj

I. INTRODUCTION

It is well known that the resonances are the most striking phenomenon in the whole range of scattering experiments, and appear widely in atomic, molecular, nuclear physics, and in chemical reactions. One of the best-known examples is the spontaneous positron production in uranium nuclei collisions, where some harp resonance peaks have been observed [1].

To explore the resonances, many techniques have been developed, which include the R-matrix theory [2], K-matrix theory [3], the scattering phase shift method [4], and several bound-state-like methods, such as the real stabilization method (RSM) [5], the analytic continuation in the coupling constant (ACCC) method [6], and the complex scaling method (CSM) [7,8]. Due to the simplicity of the calculations, these bound-state-like methods have been widely employed to study resonances in quantum many-body systems. For example, much effort has been made to more efficiently calculate resonance parameters with the RSM [9–12]. Combined with the cluster model, the ACCC approach has been used to calculate the resonances in some light nuclei [13,14]. In combination with the relativistic mean-field (RMF) theory [15–17], the RMF-ACCC has presented a good description for the structure of resonant levels in some realistic nuclei [18,19]. Moreover, the CSM have been successfully used to study resonances in atomic and molecular systems [20,21] and atomic nuclei [22–26].

Recently, the Morse potential [27] has attracted additional attention for its success in describing the motion of atomic and molecular as well as nuclear systems. The vibration of a diatomic molecule was well depicted by the Morse potential [28]. The Morse potential is also very useful in expressing the properties of nuclei [29–31]. Other applications of Morse potential include the description of the interactions between two atoms in a diatomic molecule [32–35], the interatomic potential of crystalline solids [36], and the potential for the adsorption of a molecule or atom by a solid surface [37]. This list is far from comprehensive and new applications continue to be found as well.

Due to the wide applicability, it is interesting to probe the resonances in a Morse potential. Several methods have been developed to study the resonant states of a nonrelativistic particle in a Morse potential. Nasser *et al.* [38] have adopted the J-matrix method to examine not only the bound states but also resonances associated with the rotating Morse potential model. Satpathy *et al.* [39–42] have employed the long-ranged Morse potential between two carbon nuclei in order to obtain many vibrational states which can be compared with observed resonance levels. Kato and Abe [43] have applied the Morse potential model to the ^{12}C-^{12}C system as a typical example of the molecular resonances observed in many lighter heavy-ion collisions. Jarukanont *et al.* [44] have applied the Floquet theory in combination with the exterior complex scaling to obtain the energies and the distributions of probability for the quasibound states of a driven Morse potential.

In addition to these nonrelativistic studies, much attention has been paid to the problem of the relativistic Morse potential. In 2001, the s-wave Dirac-Morse problem was formulated and solved exactly [45]. As there are no analytical solutions to the Dirac equation with $\kappa \neq 0$ for the rotational Morse potential, some approximations are employed to present the numerical or quasianalytical solutions [46,47]. To recognize the relativistic effects of the Morse potential, the Dirac equation has been solved for attractive scalar and repulsive vector Morse potentials under pseudospin symmetry by the Pekeris approximation [48,49]. Other interesting work includes the solution of the relativistic Morse potential problem under the condition of pseudospin symmetry [29].

These relativistic studies on Morse potential are associated with an interesting concept, pseudospin symmetry (PSS). The concept was first introduced in the field of nuclear physics more than 40 years ago [50,51]. Its meaning is that the single-particle states with quantum numbers $(n,l,j = l + 1/2)$ and $(n - 1, l + 2, j = l + 3/2)$ are nearly degenerate. In 1997, Ginocchio pointed out that this symmetry is a relativistic symmetry and presented the condition of exact pseudospin symmetry [52]. Afterwards, the condition of exact PSS was extended to a more general case [53], and found to be approximately satisfied in exotic nuclei with highly diffuse potentials [54]. The dynamical character of the symmetry was recognized in Ref. [55] and the spin symmetry in the antinucleon spectrum was indicated in Ref. [56]. Recent progress

---

*jianyou@ahu.edu.cn

includes the supersymmetric description for deformed nuclei [57], the nonperturbation nature of PSS [58,59], the relativistic effect of PSS [60], the influence of tensor interaction on PSS [61,62], the role of central Coulomb potential at PSS [63], and the spin and pseudospin symmetries of the Dirac equation with confining central potentials [64]. In Ref. [65], the similarity renormalization group is used as a critical tool for understanding the origin of the PSS, and the reason why the PSS becomes better for the levels closer to the continuum is disclosed in a quantitative way [66]. In combination with the supersymmetric quantum mechanics, the origin of the PSS and its breaking mechanism are detailedly analyzed at the nonrelativistic limit [67]. This symmetry is also checked in the resonant states with similar features to bound states indicated in Refs. [68,69], where it was indicated that in conditions of pseudospin symmetry the same pseudospin quantum numbers will be conserved and the pseudospin doublets would have the same energy and width. As this interesting phenomenon also appears in the resonant states, in this work we will apply the CSM to study the resonance states of a Dirac particle populating in the Morse potential, and survey the existence of PSS for this system.

II. THEORY

The Dirac equation for describing a particle moving in the Morse potential $V(r)$ is

$$H(r)\psi(r) = \begin{pmatrix} V + M & -\frac{d}{dr} + \frac{-1+\kappa}{r} \\ \frac{d}{dr} + \frac{1+\kappa}{r} & V - M \end{pmatrix} \begin{pmatrix} f(r) \\ g(r) \end{pmatrix}$$
$$= \varepsilon \begin{pmatrix} f(r) \\ g(r) \end{pmatrix} \tag{1}$$

with

$$V(r) = V_0 e^{-(r-r_0)\alpha}(2 - e^{-(r-r_0)\alpha}), \tag{2}$$

where $\kappa = \pm(j + 1/2)$ for $j = l \mp 1/2$, V_0 is the strength of the potential (or the dissociation energy in the context of diatomic molecules), r_0 is the equilibrium intermolecular distance, and α is the positive number controlling the decay length of the potential. For $V_0 < 0$, this potential has a minimum of V_0 at $r = r_0$ and it is called the regular Morse potential. For $V_0 > 0$, it has a maximum of V_0 there and it is called the inverted Morse potential, and then r_0 is the location of the top of the barrier.

The starting point of the CSM is a transformation of the Hamiltonian H, which is operated by defining an unbounded nonunitary scaling operator $U(\theta)$ with a real parameter θ. Similar to Refs. [25,70], the complex scaling operator takes the form

$$U(\theta) = \begin{pmatrix} e^{i\theta\hat{S}} & 0 \\ 0 & e^{i\theta\hat{S}} \end{pmatrix}, \tag{3}$$

where $\hat{S} = r\frac{\partial}{\partial r}$. Then, the Dirac Hamiltonian in Eq. (1) becomes a complex scaling form:

$$H_\theta = U(\theta) H U(\theta)^{-1}$$
$$= \begin{pmatrix} V(re^{i\theta}) + M & e^{-i\theta}\left(-\frac{d}{dr} + \frac{-1+\kappa}{r}\right) \\ e^{-i\theta}\left(\frac{d}{dr} + \frac{1+\kappa}{r}\right) & V(re^{i\theta}) - M \end{pmatrix}. \tag{4}$$

The corresponding complex scaled equation is

$$H_\theta\psi_\theta(r) = \varepsilon_\theta\psi_\theta(r), \tag{5}$$

where $\psi_\theta = U(\theta)\psi(r)$ is the complex scaled wave function. According to the Aguilar-Balslev-Combes theorem [71], the energy for the bound states is independent of θ, and the real part E_r and the imaginary E_i part of the energy ε_θ for the resonant states are independent of θ as well. $\Gamma = -2E_i$ represents the width for the resonant states.

In this work, Eq. (5) is solved by expanding the large and small components of the Dirac spinors $f(r)$ and $g(r)$ in terms of the radial functions $R_{nl}(r)$ of a spherical harmonic oscillator potential, i.e.,

$$f_\theta(r) = \sum_{n=1}^{n_{\max}} f_n(\theta)R_{nl}(r); \quad g_\theta(r) = \sum_{n=1}^{\tilde{n}_{\max}} g_{\tilde{n}}(\theta)R_{\tilde{n}\tilde{l}}(r), \tag{6}$$

where the orbital angular momenta l and $\tilde{l}$ have the same meaning as that in Ref. [72]. The upper limits $n_{\max}$ and $\tilde{n}_{\max}$ in Eq. (6) are radial quantum numbers determined by the corresponding major shell quantum numbers $N_{\max} = 2(n_{\max} - 1) + l$ and $\tilde{N}_{\max} = 2(\tilde{n}_{\max} - 1) + \tilde{l}$. In the present calculations, the maximum of the major shell quantum number $N = 200$ is chosen to ensure the calculated result with the accuracy better than the order of 10^{-4} fm^{-2} or 10^{-4} a.u. for the energies and widths. The details can be referred to in the literature [70,72].

Inserting Eq. (6) into Eq. (5) and using the orthogonality of wave functions R_{nl}, one arrives at a symmetric matrix diagonalization problem of the dimension $n_{\max} + \tilde{n}_{\max}$, i.e.,

$$\begin{pmatrix} V_{n,n'} + M\delta_{n,n'} & B_{n,\tilde{n}'} \\ B_{\tilde{n},n'} & V_{\tilde{n},\tilde{n}'} - M\delta_{\tilde{n},\tilde{n}'} \end{pmatrix} \begin{pmatrix} f_{n'} \\ g_{\tilde{n}'} \end{pmatrix} = \varepsilon_\theta \begin{pmatrix} f_n \\ g_{\tilde{n}} \end{pmatrix}. \tag{7}$$

The matrix elements $V_{n,n'}$ and $B_{n,\tilde{n}'}$ are given by

$$V_{n,n'} = \int_0^\infty r^2 dr \, R_{nl}(r)[V(re^{i\theta})]R_{n'l}(r), \tag{8}$$

$$B_{\tilde{n},n'} = e^{-i\theta}\int_0^\infty r^2 dr \left[R_{\tilde{n}\tilde{l}}(r)\left(\frac{d}{dr} + \frac{1+\kappa}{r}\right)R_{n'l}(r)\right]. \tag{9}$$

The integral in Eq. (8) is calculated with the Gauss quadrature approximation [20,70]. The matrix elements $B_{n,\tilde{n}'}$ can be further simplified as

$$B_{\tilde{n},n'} = \begin{cases} -\frac{1}{b_0e^{i\theta}}(\sqrt{\tilde{n}+l+1/2}\delta_{\tilde{n},n'} + \sqrt{\tilde{n}}\delta_{\tilde{n},n'-1}), & \kappa < 0 \\ \frac{1}{b_0e^{i\theta}}(\sqrt{\tilde{n}+l-1/2}\delta_{\tilde{n},n'} + \sqrt{\tilde{n}-1}\delta_{\tilde{n},n'+1}), & \kappa > 0. \end{cases} \tag{10}$$

With the matrix elements $V_{\tilde{n}\tilde{n}'}$ and $B_{n,\tilde{n}'}$, the solutions of the Dirac equation are obtained by diagonalizing the matrix

$$H_\theta = \begin{pmatrix} V_{n,n'} + M\delta_{n,n'} & B_{n,\tilde{n}'} \\ B_{\tilde{n},n'} & V_{\tilde{n},\tilde{n}'} - M\delta_{\tilde{n},\tilde{n}'} \end{pmatrix}. \tag{11}$$

The eigenvalues of H_θ representing the bound or resonant states do not change with θ, while eigenvalues representing the continuous spectrum rotate.
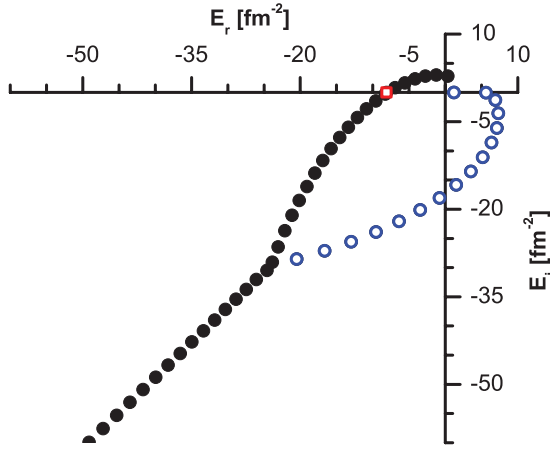
FIG. 1. (Color online) Position in complex energy surface for the states with $\kappa = -1$, where the bound, the resonant, and the continuum are respectively labeled as open boxes, open circles, and solid circles. The parameters in the Morse potential are adopted as $V_0 = 6$ fm^{-2}, $r_0 = 4$ fm, and $\alpha = 0.3$ fm^{-1}. The mass of particle $M = 0.5$ fm^{-1} and the rotation angle $\theta = 70°$ are adopted in the present calculations.

III. RESULT AND DISCUSSION

With the theoretical formalism represented in the previous section, we explore the resonant states for a particle populating in a Morse potential. For comparison with the results from the J-matrix approach in Ref. [38], the same values for the parameters of the Morse potential are employed. The illustrated results are plotted in Fig. 1 with the complex rotation angle $\theta = 70°$ for the states with $\kappa = -1$. It should be mentioned that the energy displayed in Fig. 1 is multiplied by a factor $2M/\hbar^2$ in order to compare with Ref. [38]. The same as Fig. 1, the energy and the depth of potential in the following Table I and Figs. 2 and 3 are multiplied by a factor $2M/\hbar^2$.

All the eigenvalues of H_θ, which correspond to the bound, resonant, and continuum states, are respectively labeled as open boxes, open circles, and solid circles. From Fig. 1, one sees clearly that the eigenvalues of H_θ fall into three regions: The bound states populate on the negative energy axis, while the continuous spectrum of H_θ rotates clockwise with the angle 2θ, and resonances in the lower half of the complex energy plane located in the sector bound by the new rotated cut line and the positive energy axis get exposed and become isolated. In the present calculations, as the finite basis is used, the continuous spectrum of H_θ consists of a string of points.

The energies for the resonant states in Fig. 1 are listed in Table I. The relativistic results are shown in the first column. The second column displays the data in the nonrelativistic limit, which are obtained with an approximation by increasing the value of the speed of light up to 100 times larger than its actual value in the relativistic CSM calculations [20]. In order to compare with the other methods, some data from the nonrelativistic calculations are exhibited in the third column by the J-matrix method [38] and the fourth column by the S-matrix method [73]. From Table I, it can be seen that the deviation between the relativistic result and that in the nonrelativistic limit is observable, which implies the relativistic effect cannot be completely ignored in the present model. The present calculations in the nonrelativistic limit agree with the nonrelativistic calculations quite well. The deviation between our results and the data by the J-matrix or S-matrix method is very small. Whether for a relativistic or nonrelativistic system, the present method has provided a good description for the resonant states. Hence, we can look into all the resonant states for a Dirac particle in a Morse potential by this method.

To survey the resonances in a wider range, it is necessary to analyze the dependence of the resonant parameters on the shape of the potential, which can help us to recognize

TABLE I. Energies in the present calculations for the states with $\kappa = -1$ in comparison with the data in Refs. [38,73]. Here the parameters of Morse potential are adopted as $V_0 = 6$ fm^{-2}, $r_0 = 4$ fm, and $\alpha = 0.3$ fm^{-1}. The mass of particle is adopted as $M = 0.5$ fm^{-1}. For comparison with Refs. [38,73], the depth of potential displayed and the calculated energies are multiplied by a factor $2M/\hbar^2$.

| $E_r + iE_i$ (fm^{-2}) Relativistic	$E_r + iE_i$ (fm^{-2}) Nonrelativistic limit	$E_r + iE_i$ (fm^{-2}) Nasser [38]	$E_r + iE_i$ (fm^{-2}) Rawitscher [73]
-8.1096	-8.1089	-8.1090	-8.1090
$1.1745 - i\,0.0002$	$1.1779 - i\,0.0011$	$1.1778 - i\,2.01\times10^{-13}$	1.1783
$5.6229 - i\,0.0349$	$5.6212 - i\,0.0303$	$5.6252 - i\,0.0351$	$5.6252 - i\,0.0351$
$6.8906 - i\,1.3170$	$6.9041 - i\,1.3103$	$6.8911 - i\,1.3194$	
$7.3194 - i\,3.5858$	$7.3375 - i\,3.6189$	$7.3182 - i\,3.5887$	
$7.1143 - i\,6.0693$	$7.0545 - i\,6.0853$	$7.1111 - i\,6.0715$	
$6.3679 - i\,8.5999$	$6.3820 - i\,8.5374$	$6.3627 - i\,8.6005$	
$5.1514 - i\,11.0980$	$5.1806 - i\,11.1429$	$5.1446 - i\,11.0960$	
$3.5200 - i\,13.5209$	$3.4649 - i\,13.5147$	$3.5123 - i\,13.5151$	
$1.5173 - i\,15.8439$	$1.5262 - i\,15.8071$	$1.5095 - i\,15.8334$	
$-0.8212 - i\,18.0518$	$-0.8167 - i\,18.0490$	$-0.8278 - i\,18.0358$	
$-3.4656 - i\,20.1350$	$-3.4773 - i\,20.1177$	$-3.4697 - i\,20.1128$	
$-6.3907 - i\,22.0869$	$-6.3930 - i\,22.0537$	$-6.3907 - i\,22.0579$	
$-9.5750 - i\,23.9031$	$-9.5671 - i\,23.8658$	$-9.5691 - i\,23.8667$	
$-12.9998 - i\,25.5801$	$-12.9859 - i\,25.5370$	$-12.9861 - i\,25.5363$	
$-16.6491 - i\,27.1155$	$-16.6258 - i\,27.0640$	$-16.6255 - i\,27.0642$	
$-20.5088 - i\,28.5077$	$-20.4731 - i\,28.4487$		
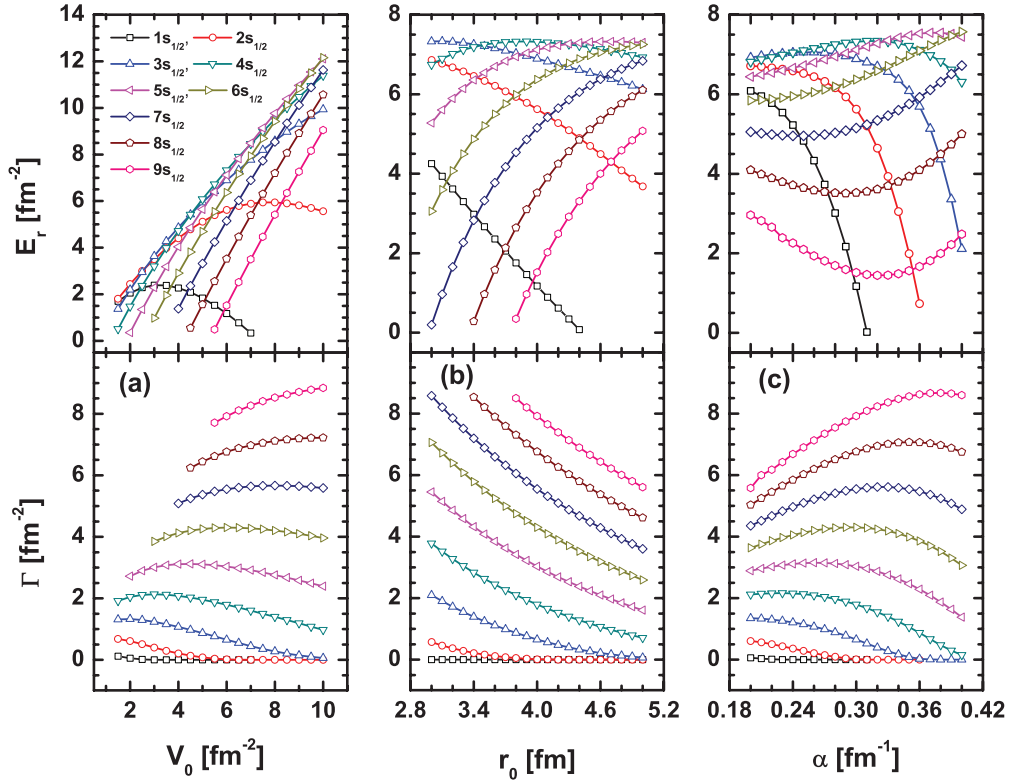
FIG. 2. (Color online) Energies and widths as a function of every potential parameter for the resonant states shown in Fig. 1. The data corresponding to the variables V_0, r_0, and α are respectively displayed in (a), (b), and (c) with the other parameters fixed to $r_0 = 4$ fm, $\alpha = 0.3$ fm^{-1} in (a), $V_0 = 6$ fm^{-2}, $\alpha = 0.3$ fm^{-1} in (b), and $V_0 = 6$ fm^{-2}, $r_0 = 4$ fm in (c). The mass of particle is adopted as $M = 0.5$ fm^{-1}.

the resonances for more realistic systems. The variations of energy and width with the parameters of the potential are shown in Fig. 2, where the data associated with the dissociation energy, the equilibrium intermolecular distance, and the positive number controlling the decay length of

FIG. 3. (Color online) The Morse potential model for (a) various strength of the potential $V_0 = 1, 6, 10$ fm^{-2} along with $r_0 = 4$ fm and $\alpha = 0.3$ fm^{-1}; (b) various equilibrium intermolecular distance $r_0 = 3, 4, 5$ fm along with $V_0 = 6$ fm^{-2} and $\alpha = 0.3$ fm^{-1}; and (c) various positive number $\alpha = 0.2, 0.3, 0.4$ fm^{-1} along with $V_0 = 6$ fm^{-2} and $r_0 = 4.0$ fm.

the potential are respectively shown in the panels (a), (b), and (c) of Fig. 2. Starting from $V_0 = 1.5$ fm^{-2}, the energy of the resonant states increases with the increasing of V_0. Further increasing V_0, the energy level changes the direction of evolution for the $1s_{1/2}$, followed by the $2s_{1/2}$, and so on. Simultaneously, some new resonant levels are exposed. For the width, its evolution with V_0 is consistent with that for the energy. Starting from $V_0 = 1.5$ fm^{-2}, the width reduces with the increasing V_0 for the several lower levels. For the several upper levels, the width increases with the increasing V_0. As n increases, the width is sequentially changed in the direction of the evolution with V_0. The phenomenon can be explained by the potential energy curves plotted in Fig. 3. With the increase of V_0, the barrier becomes higher and the well becomes deeper
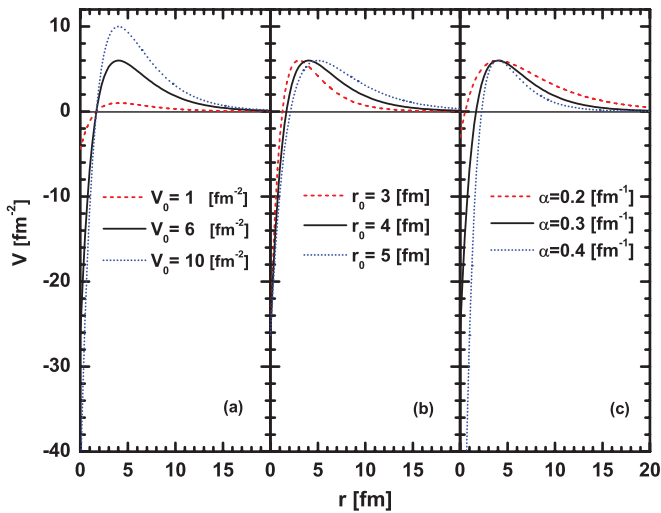
TABLE II. The same as Table I, but for the states with $\kappa = 2$ in comparison with the data in Ref. [38]. Here the parameters of Morse potential are adopted as $V_0 = 10$, $r_0 = 1$, and $\alpha = 2.0$ in the atomic units $\hbar = m = 1$.

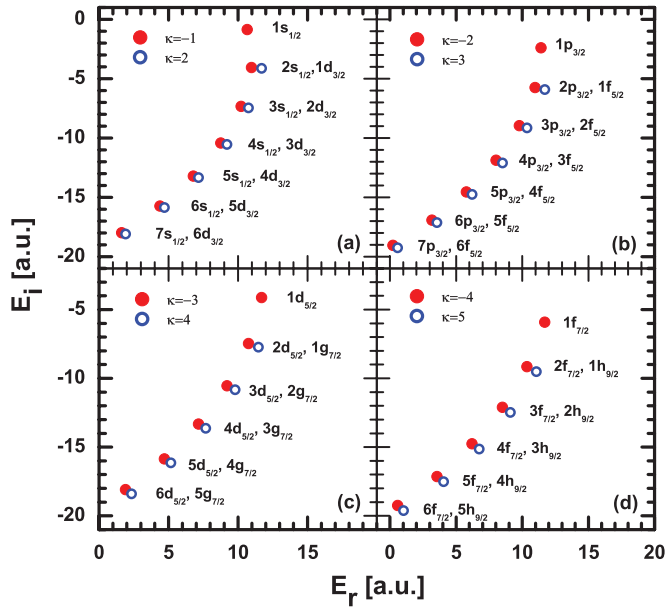| $E_r + i E_i$ Relativistic	$E_r + i E_i$ Nonrelativistic limit	$E_r + i E_i$ Nasser [38]
−30.7047	−30.4136	−30.4139
10.8020 −i 0.2822	10.9262 −i 0.3026	10.9260 −i 0.3027
17.1419−i 12.3689	17.1244 −i 12.5031	17.1240 −i 12.5027
11.1795 −i 32.0868	11.0511 −i32.1914	11.0521 −i 32.1906
−4.8377 −i 52.5443	−5.0383 −i 52.5395	−5.0376 −i 52.5407
−29.3283 −i 72.2381	−29.5208 −i 72.0565	

FIG. 4. (Color online) Pseudospin doublets in the complex energy surface for the Morse potential with the parameters $V_0 = 10$, $r_0 = 1$, and $\alpha = 0.5$ in the atomic units $\hbar = m = 1$.

as seen in Fig. 3(a) for the Morse potential. It is the reason that the resonant parameters vary with V_0 in accordance with the foregoing. With the increase of n, the evolution of the resonant energy with r_0 changes from a decrease to an increase with the

increasing r_0. At the level located in the middle, the energy of the state ($4s_{1/2}$) only has a slight change. The energy for the levels lower than $4s_{1/2}$ decreases with the increasing r_0, while the energy increases with the increasing r_0 for the energy level populating in higher than $4s_{1/2}$, which is associated with the variation of the potential. From the potential energy curves in Fig. 3(b), one can see that both the barrier and the well become wider with the increase of r_0, which leads to a weakening of penetration for a particle in the Morse potential. Thus, the width becomes systematically smaller with the increasing r_0. Figure 2(c) shows the resonant parameters varying with α; a similar change is seen for the energy with r_0 in Fig. 2(b) and for the width with V_0 in Fig. 2(a). These can be explained from the changes in the potential field. The potential energy curves in Fig. 3(c) display that the potential well becomes deeper and the range of the potential barrier becomes narrower with the increase of α, which is the cause of the resonant parameters with α.

To further examine the present CSM calculations, the resonant states with $\kappa = 2$ is investigated with the data exhibited in Table II. For comparisons with the data in Ref. [38], the atomic units $\hbar = m = 1$ are adopted here. Similar to Table I, the result in the nonrelativistic limit is obtained according to the method in Ref. [20]. From Table II, it can be seen our results are in excellent agreement with the data in Ref. [38], which are obtained by the J-matrix method for a nonrelativistic system. These show the present calculations are fully correct, and we can explore the resonant states of a relativistic particle by this method.
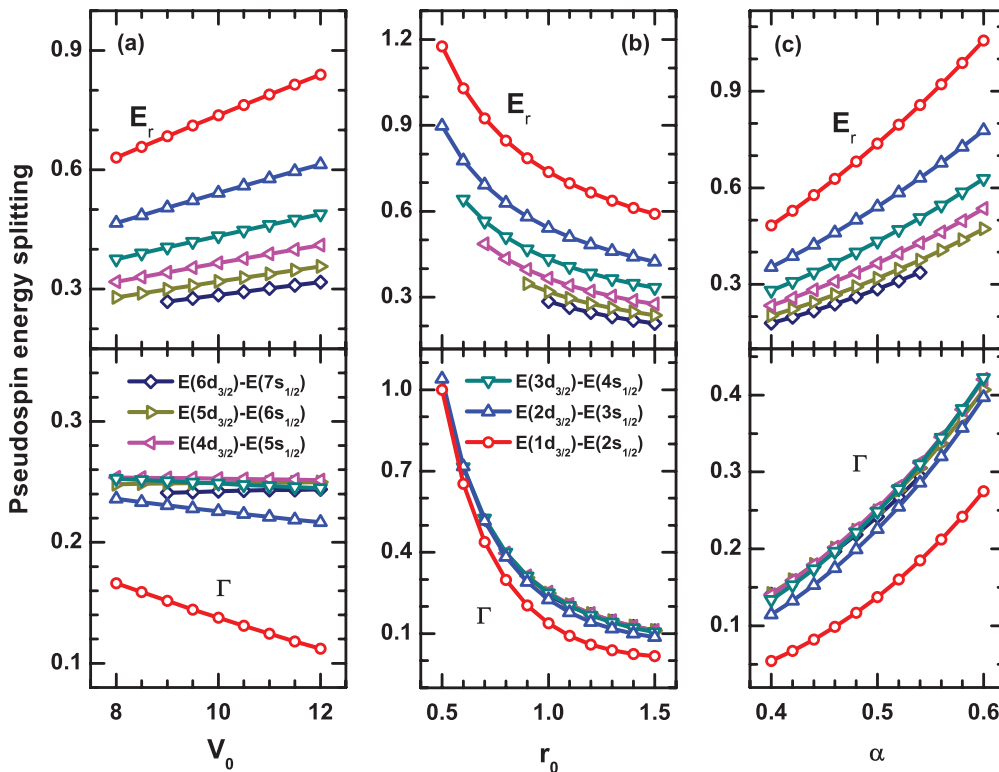

FIG. 5. (Color online) Pseudospin energy and width splittings as a function of every potential parameter for the resonant states shown in Fig. 4(a). The data corresponding to the variables V_0, r_0, and α are respectively displayed in (a), (b), and (c) with the other parameters fixed to $r_0 = 1$, $\alpha = 0.5$ in (a), $V_0 = 10$, $\alpha = 0.5$ in (b), and $V_0 = 10$, $r_0 = 1$ in (c) in the atomic units $\hbar = m = 1$.

With the resonance states obtained by the CSM, the position of pseudospin doublets in the complex energy surface is shown in Fig. 4, where the pseudospin doublets $\kappa = -1$ and 2, $\kappa = -2$ and 3, $\kappa = -3$ and 4, as well as $\kappa = -4$ and 5 are respectively displayed in Figs. 4(a)–4(d). It is clear that PSS is well preserved for all the doublets. For the pseudospin doublet with the same orbital angular momentum, the quality of PSS improves with the increase of the radial quantum number.

To disclose the relationship of the PSS in the resonant states and the shape of the potential, we analyze the variation of the pseudospin splittings with the parameters in the Morse potential. Keeping r_0 and α fixed, we vary V_0 to see how the energy and width of the pseudospin doublets are sensitive to the dissociation energy. This dependence is shown in Fig. 5(a) for the energy and width splitting. It is clear that the energy splitting of the pseudospin doublets increases with the increase of V_0, while an inverse trend is found for the variation of width. This can be easily understood as higher barrier and deeper potential well are accompanied with the increase of V_0. Similarly, the energy and width splittings varying with r_0 are displayed in Fig. 5(b) with the other parameters fixed. From the left ($r_0 = 0.5$), as the radius r_0 increases, the energy and width splittings decrease, which can be understood by the dependence of $dV(r)/dr$ on r. The variation of the pseudospin splittings with α is presented in Fig. 5(c). For all the pseudospin doublets, the tendency for the change of the pseudospin energy and width splittings with α is the same. With α increases, the splitting increases. This could be expected because the potential well becomes deeper and widened with the increase of α, hence the increase of the derivative of $V(r)$. In the range of the potential parameters considered here, the deviations between pseudospin doublets are within 1.17 a.u. for E_r and 1.04 a.u. for Γ, which indicates the PSS is well preserved.

IV. SUMMARY

In summary, the resonant states of Morse potential are investigated by using the complex scaling method in the relativistic framework. The calculated results are compared with the available data in references and satisfactory agreements are found. Further, the dependence of the resonant parameters on the shape of the potential is checked and a unified result is found for the evolution of the resonant parameters with the potential parameters, which can be well explained from the change of potential energy curves. With these resonant states obtained, the PSS in the resonant states is investigated and well PSS is found in the present model. The pseudospin splitting is shown in correlation with the Morse potential shaped by the dissociation energy V_0, the equilibrium intermolecular distance r_0, and the positive number controlling the decay length of the potential α, in which three Morse potential parameters V_0, α, and r_0 are found to play the important roles in the splittings of energy and width of pseudospin doublets.

[1] T. Cowan *et al.*, Phys. Rev. Lett. **56**, 444 (1986).

[2] G. M. Hale, R. E. Brown, and N. Jarmie, Phys. Rev. Lett. **59**, 763 (1987).

[3] J. Humblet, B. W. Filippone, and S. E. Koonin, Phys. Rev. C **44**, 2530 (1991).

[4] J. R. Taylor, *Scattering Theory: The Quantum Theory on Nonrelativistic Collisions* (Wiley, New York, 1972).

[5] A. U. Hazi and H. S. Taylor, Phys. Rev. A **1**, 1109 (1970).

[6] V. I. Kukulin, V. M. Krasnopolsky, and J. Horáček, *Theory of Resonances: Principles and Applications* (Kluwer Academic, Dordrecht, 1989).

[7] Y. K. Ho, Phys. Rep. **99**, 1 (1983).

[8] N. Moiseyev, Phys. Rep. **302**, 212 (1998).

[9] H. S. Taylor and A. U. Hazi, Phys. Rev. A **14**, 2071 (1976).

[10] V. A. Mandelshtam, H. S. Taylor, V. Ryaboy, and N. Moiseyev, Phys. Rev. A **50**, 2764 (1994).

[11] A. T. Kruppa and K. Arai, Phys. Rev. A **59**, 3556 (1999).

[12] L. Zhang, S. G. Zhou, J. Meng, and E. G. Zhao, Phys. Rev. C **77**, 014312 (2008).

[13] N. Tanaka, Y. Suzuki, and K. Varga, Phys. Rev. C **56**, 562 (1997).

[14] N. Tanaka, Y. Suzuki, K. Varga, and R. G. Lovas, Phys. Rev. C **59**, 1391 (1999).

[15] S. C. Yang, J. Meng, and S. G. Zhou, Chin. Phys. Lett. **18**, 196 (2001).

[16] S. S. Zhang, J. Meng, S. G. Zhou, and G. C. Hillhouse, Phys. Rev. C **70**, 034308 (2004).

[17] S. S. Zhang, M. S. Smith, G. Arbanas, and R. L. Kozub, Phys. Rev. C **86**, 032802(R) (2012).

[18] J. Y. Guo, R. D. Wang, and X. Z. Fang, Phys. Rev. C **72**, 054319 (2005).

[19] J. Y. Guo and X. Z. Fang, Phys. Rev. C **74**, 024320 (2006).

[20] A. D. Alhaidari, Phys. Rev. A **75**, 042707 (2007).

[21] M. Bylicki, G. Pestka, and J. Karwowski, Phys. Rev. A **77**, 044501 (2008).

[22] A. T. Kruppa, P.-H. Heenen, H. Flocard, and R. J. Liotta, Phys. Rev. Lett. **79**, 2217 (1997).

[23] K. Arai, Phys. Rev. C **74**, 064311 (2006).

[24] T. Myo, Y. Kikuchi, and K. Kato, Phys. Rev. C **85**, 034338 (2012), and references therein.

[25] J. Y. Guo, X. Z. Fang, P. Jiao, J. Wang, and B. M. Yao, Phys. Rev. C **82**, 034318 (2010).

[26] Q. Liu, J. Y. Guo, Z. M. Niu, and S. W. Chen, Phys. Rev. C **86**, 054312 (2012).

[27] P. M. Morse, Phys. Rev. **34**, 57 (1929).

[28] M. E. Goggin and P. W. Milonni, Phys. Rev. A **37**, 796 (1988).

[29] O. Aydoğdu and R. Sever, Phys. Lett. B **703**, 379 (2011).

[30] I. Inci, D. Bonatsos, and I. Boztosun, Phys. Rev. C **84**, 024309 (2011).

[31] I. Boztosun, D. Bonatsos, and I. Inci, Phys. Rev. C **77**, 044302 (2008).

[32] D. A. Morales, Chem. Phys. Lett. **161**, 253 (1989).

[33] E. D. Filho and R. M. Ricotta, Phys. Lett. A **269**, 269 (2000).

[34] J. P. Killingbeck, A. Grosjean, and G. Jolicard, J. Chem. Phys. **116**, 447 (2002).

[35] S. H. Dong, R. Lemus, and A. Frank, Int. J. Quantum Phys. **86**, 433 (2002).

[36] K. Mohammed, M. M. Shukla, F. Milstein, and J. L. Merz, Phys. Rev. B **29**, 3117 (1984).

[37] J. T. Sun, L. Gao, X. B. He, Z. H. Cheng, Z. T. Deng, X. Lin, H. Hu, S. X. Du, F. Liu, and H. J. Gao, Phys. Rev. B **83**, 115419 (2011).

[38] I. Nasser, M. S. Abdelmonem, H. Bahlouli, and A. D. Alhaidari, J. Phys. B **41**, 215001 (2008).

[39] L. Satpathy and P. Sarangi, J. Phys. G **16**, 469 (1990).

[40] L. Satpathy, Prog. Part. Nucl. Phys. **29**, 327 (1992).

[41] L. Satpathy and P. Sarangi, J. Phys. G **20**, L37 (1994).

[42] L. Satpathy, J. Phys. G **31**, 1233 (2005).

[43] K. Kato and Y. Abe, Phys. Rev. C **55**, 1928 (1997).

[44] D. Jarukanont, K. Na, and L. E. Reichl, Phys. Rev. A **75**, 023403 (2007).

[45] A. D. Alhaidari, Phys. Rev. Lett. **87**, 210405 (2001).

[46] S. Flugge, *Practical Quantum Mechanics* (Springer-Verlag, Berlin, 1974).

[47] F. Cooper, A. Khare, and U. Sukhatme, *Supersymmetry in Quantum Mechanics* (World Scientific, Singapore, 2001).

[48] C. Berkdemir, Nucl. Phys. A **770**, 32 (2006).

[49] W. C. Qiang, R. S. Zhou, and Y. Gao, J. Phys. A: Math. Theor. **40**, 1677 (2007).

[50] K. T. Hecht and A. Adler, Nucl. Phys. A **137**, 129 (1969).

[51] A. Arima, M. Harvey, and K. Shimizu, Phys. Lett. B **30**, 517 (1969).

[52] J. N. Ginocchio, Phys. Rev. Lett. **78**, 436 (1997).

[53] J. Meng, K. Sugawara-Tanabe, S. Yamaji, P. Ring, and A. Arima, Phys. Rev. C **58**, R628 (1998).

[54] J. Meng, K. Sugawara-Tanabe, S. Yamaji, and A. Arima, Phys. Rev. C **59**, 154 (1999).

[55] P. Alberto, M. Fiolhais, M. Malheiro, A. Delfino, and M. Chiapparini, Phys. Rev. Lett. **86**, 5015 (2001).

[56] S. G. Zhou, J. Meng, and P. Ring, Phys. Rev. Lett. **91**, 262501 (2003).

[57] A. Leviatan, Phys. Rev. Lett. **103**, 042502 (2009).

[58] H. Z. Liang, P. W. Zhao, Y. Zhang, J. Meng, and N. V. Giai, Phys. Rev. C **83**, 041301(R) (2011).

[59] J. N. Ginocchio, J. Phys. Conf. Ser. **267**, 012037 (2011).

[60] S. W. Chen and J. Y. Guo, Phys. Rev. C **85**, 054312 (2012).

[61] W. H. Long, P. Ring, J. Meng, N. Van Giai, and C. A. Bertulani, Phys. Rev C **81**, 031302(R) (2010).

[62] L. B. Castro, Phys. Rev. C **86**, 052201(R) (2012).

[63] A. S. de Castro and P. Alberto, Phys. Rev. A **86**, 032122 (2012).

[64] P. Alberto, A. S. de Castro, and M. Malheiro, Phys. Rev. C **87**, 031301(R) (2013).

[65] J. Y. Guo, Phys. Rev. C **85**, 021302(R) (2012).

[66] D. P. Li, S. W. Chen, and J. Y. Guo, Phys. Rev. C **87**, 044311 (2013).

[67] H. Z. Liang, S. H. Shen, P. W. Zhao, and J. Meng, Phys. Rev. C **87**, 014334 (2013).

[68] B. N. Lu, E. G. Zhao, and S. G. Zhou, Phys. Rev. Lett. **109**, 072501 (2012).

[69] B. N. Lu, E. G. Zhao, and S. G. Zhou, arXiv:1303.0630.

[70] J. Y. Guo, M. Yu, J. Wang, B. M. Yao, and P. Jiao, Comput. Phys. Commun. **181**, 550 (2010).

[71] J. Aguilar and J. M. Combes, Commun. Math. Phys. **22**, 269 (1971) E. Balslev and J. M. Combes, *ibid.* **22**, 280 (1971).

[72] Y. K. Gambhir, P. Ring, and A. Thimet, Ann. Phys. (NY) **198**, 132 (1990).

[73] G. Rawitscher, C. Merow, M. Nguyen, and I. Simbotin, Am. J. Phys. **70**, 935 (2002).